Chemical Physics Impact 8 (2024) 100495

Contents lists available at ScienceDirect

Chemical Physics Impact

journal homepage: www.sciencedirect.com/journal/chemical-physics-impact

Full Length Article

Quantum chemical and MD investigations on molecular structure, vibrational (FT-IR and FT-Raman), electronic, thermal, topological, molecular docking analysis of 1-carboxy-4-ethoxybenzene

C.P. Devipriya [a,b,1], S. Deepa [c], J. Udayaseelan [b], RaviKumar Chandrasekaran [d], M. Aravinthraj [e,*], V. Sabari [a,1,*]

[a] PG and Research Department of Physics, Marudhar Kesari Jain College for Women (Autonomous), Vaniyambadi 635 751, Tamil Nadu, India
[b] PG and Research Department of Physics, Government Thirumagal Mills College, Gudiyatham 635 803, Tamil Nadu, India
[c] Department of Physics, Government College of Engineering, Salem 636 011, Tamil Nadu, India
[d] Department of Physics, Thanthai Periyar E V R Government Polytechnic College, Vellore 632 002, Tamil Nadu, India
[e] PG and Research Department of Physics, Sacred Heart College (Autonomous), Tirupattur 635 601, Tamil Nadu, India

ARTICLE INFO

Keywords:
FT-IR
FT-Raman
Topological properties
Molecular docking
Molecular dynamics

ABSTRACT

The current study focuses on the combined experimental and theoretical FT-IR and FT-Raman spectra of 1-carboxy-4-ethoxybenzene (1C4EB), to obtain vibrational frequencies and optimal geometrical parameters by HF and DFT. For 1C4EB, the kind of intramolecular interactions and their stabilization were performed by Natural Bond Orbital analysis. The Nonlinear optical p properties and the conclusive evidence for ICT were also analyzed. The electronic energies and absorption spectra in different mediums were determined. Furthermore, Mulliken charges distribution, molecular electrostatic potential maps, the condensed Fukui function and thermodynamic parameters were calculated. The topological properties and IRI were analyzed with the Multiwfn program. In molecular docking, target proteins 4ULE and 2EEP were used to investigate sugar phosphatase and Prolyl aminopeptidase inhibitor properties. The least binding energy -6.7 kcal/mol is observed for the selected protein 4ULE. The molecular dynamics of the complex between the proteins 4ULE and 2EEP – ligand, binding free energies also calculated by the Poisson-Boltzmann surface area method.

Introduction

There are plenty of uses for the aromatic carboxylic acids attracted researchers for their reliabilities in many applications [1]. In particular, benzoic acid with its substituents plays the inevitable role in treating fungal diseases by controlling yeast formation and bacterial growth, benzoic acid liniments are also used as neuraminidase inhibitors against cancer and influenza, characterized by their antifungal and antibacterial properties [2].

Several [3–8] researchers have made extensive contributions to the analysis of aromatic carboxylic acids. Especially, some of the specific spectroscopic and quantum chemical analyses of 2, 3, 5-dimethyl-4-methoxybenzoic acid, 5-amino-2-nitrobenzoic acid, 2-(4-hydroxyphenylazo) benzoic acid [9,10], 2-chloro-5-nitrobenzoic acid, 3, 5-dinitro benzoic acid [11] and also made some remarkable researches of benzoic acid compounds in treating COVID-19 and cancer [12], which have enabled us the broad eye-opening of the present research on the selected molecule 1-carboxy-4-ethoxybenzene (1C4EB).

The rigorous literature survey made and found that 1-carboxy-4-ethoxybenzene (1C4EB) has not been investigated in quantum chemical treatment and molecular docking for the latest drug design. We analyzed the molecular structure and theoretically predicted vibrational assignments of 1C4EB compared with its experimental results, thermodynamic and Natural Bond orbital and Non-Linear Optical parameters. The attacking sites on MEP surfaces are based on nucleophilic and electrophilic reactions, the topographic evaluation of LOL, ELF, iso surface and IRI. According to Molecular docking studies, 1C4EB exerts sugar phosphatase inhibitors or prolyl aminopeptidase inhibitor properties upon interacting with selected targets and in the next step, binding free energies of enzyme-ligand complexes with the highest scores were

* Corresponding authors.
E-mail addresses: m.aravinthraj@gmail.com (M. Aravinthraj), vrsabari86@gmail.com (V. Sabari).
[1] Affiliated to Thiruvalluvar University, Serkkadu, Vellore, Tamil Nadu, India.

https://doi.org/10.1016/j.chphi.2024.100495

Available online 26 January 2024

determined by molecular dynamics simulations. Sugar- phosphatase deficiency is a class of hereditary metabolic diseases which includes types Ia and Ib, characterized by poor tolerance to fasting, growth retardation and hepatomegaly resulting from accumulation of glycogen and fat in the liver. The disease of hypoglycemia often appear between the early ages. The patients exhibit growth retardation, significant hepatomegaly, and poor tolerance to fasting. Furthermore, neutropenia and neutrophil dysfunction are responsible for tendency towards infections and inflammatory bowel disease [13,14].

Experimental studies

The 1-carboxy-4-ethoxybenzene (1C4EB) was obtained from Aldrich Chemicals with an indicated 99 % assay and used directly for the present study without purification. For the title molecule 1C4EB, the FT-IR spectrum is recorded by a Perkin Elmer Spectrum RX in between 400 and 4500 cm^{-1} with 1 cm^{-1} of resolution in the spectral domain. FT-Raman spectrum is recorded by Bruker RFS 27 enabled by Nd: YAG Laser sample excitation wavelength of 1064 nm and operating in the spectral Stokes shift in the range of region 50 to 4000 cm^{-1} respectively. The spectra are recorded in SAIF, IITM, Chennai, Tamil Nadu, India

Quantum chemical calculations

The Gaussian 09 W [15] software is employed to attain the quantum chemical calculations of 1C4EB by HF and DFT-B3LYP methods. There are two quantum chemical methods used for calculations on 1C4EB: the Hartree-Fock (HF) method, which treats electrons as non-interacting, and the Density Functional Theory with B3LYP (DFT-B3LYP) method, which combines efficiency and accuracy at the same time. In comparison with HF, DFT-B3LYP considers electron density for a comprehensive understanding of electronic structure, while HF provides a basic description of electronic structure. This study has been made more reliable by the use of both methods, providing diverse insights into the electronic properties of 1C4EB as a result of its use of both methods. [16,17]. The geometrical structure of 1C4EB and vibrational frequencies along with potential energy distributions (PED) calculations were carried out to assign vibrational spectra at minimum energy based on the level standard basis set, which is a useful tool for both qualitative and quantitative studies. The scaled frequencies of the adopted HF method are adjusted to 0.967 and for the B3LYP method are adjusted to 0.958 for wave numbers nearer to 1700 cm^{-1} and rounded to 0.9833 for wave numbers nearer to 1900 cm^{-1} [18,19]. Altering subsequent scaling factors acquired from the experimental derivation which were lesser than 10 cm^{-1}. Based on PED's calculation the Vibrational Energy Distribution Analysis (VEDA) [20] program was utilized to generate descriptions for the quantum chemical vibrational frequencies and normal modes were assigned. The visual animations of vibrational modes were created with the Gauss view 6.06 [21]. Natural Bonding Orbitals were computed using the Gaussian 09 W at the adopted B3LYP basic set [22]. Using NBO analysis, the Fukui functions of single-point energy calculations have been done for N+1 and N-1 species. The second-order perturbation approach calculates hyperconjugative interaction energy [23–25]. An electronic property such as HOMO and LUMO energy can be determined using TD-DFT. Mulliken population analysis is used to calculate a group contribution to a molecular orbital. A thermodynamic analysis of the estimated vibrational frequencies of normal mode. The topological analyses such as Electron localization function (ELF), Localized orbital locator (LOL), Molecular electrostatic potential (MEP) and Interaction Region Indicator (IRI) analyses were performed using Multiwfn 3.8 [26].

Molecular docking and dynamics simulation

A docking study of 1C4EB with selected target proteins was carried out by the Auto Dock Vina program [27] and Discovery Studio [28] was used to visualize the docking findings. The molecular Dynamics of 1C4EB is simulated by the SiBioLead online platform (https://sibiolead.com/) with sugar phosphatase inhibitor and Prolyl aminopeptidase inhibitor proteins at 300 K and a pressure of 1 bar in 0.15 M NaCl. A simulation consisted of approximately 1000 frames with a simulated time set of 1 nanosecond and calculated binding free energies by the MM-PBSA method.

Results and discussion

Molecular geometry

The relative parameters of the optimal structural like bond lengths and angles of 1C4EB based on C_S group symmetry are presented in Table S1. Berny's optimization algorithm is employed to optimize the molecular structure using Gaussian 09 W and Gauss view 6.06 as shown in Fig. 1(a). In HF and DFT with a standard basis set, the structural optimization and zero-point vibrational energies were calculated to be 118.07 and 110.12 Kcal/mol. The ground state energy in HF is more significant than the actual energy; the calculated energy of HF is greater than the DFT method. The carboxyl group is attached to the C_1-C_2, the bond length value of 1.480 Å and 1.478 Å is higher than other bond lengths. HF and DFT possess the most elevated bond angle (d, p) for C_2-C_1-O_8. Experimentally [29] measured bond lengths and angles are correlated by theoretically simulated values. Furthermore, the dimer of 1C4EB molecules showed in Fig. 1(b) the possibility of the intermolecular hydrogen bonding (O—H·····O=C) of lengths 1.572 Å and 1.586 Å, The bond angles 125° and 126° using the B3LYP basis set.

Vibrational assignments

The molecule 1C4EB had a non-planar symmetry, in total, 22 atoms are presented in it and undergoes 60 normal modes of vibrations spanning irreducible representations within the C_S group. Amongst 60 normal modes, 36 belong to in-plane bending and 24 are for out-of-plane bending. In the molecule, those bands in the plane bending are represented by A′, while A″ species represent those out of the plane, i.e., ⌈vib = 36A′ + 24 A″. The HF/DFT vibrational frequencies were computed using the optimized structural parameters at the standard basis set level. Table 1 listed the vibrational theoretical and experimental assignments of the functional groups presented in 1C4EB and their corresponding figures shown are in Figs. 2-3.

OH vibrations

The stretching frequency of hydroxyl group vibrations occurs between 3400 and 3600 cm^{-1}[30]. For 1C4EB, a significant FTIR peak at 3423 cm^{-1} assigned to OH stretching vibrations, Sajan et al. reported the same occurred at 3500 cm^{-1} [31]. Since, Intermolecular hydrogen bonding between hydroxyl and carbonyl groups of 1C4EB (ie., O—H····O=C) has slightly shifted towards. Theoretical FTIR, OH peaks were observed at 3422 cm^{-1} and 3413 cm^{-1} respectively by HF and DFT methods and no significant FT-Raman peaks were observed. From Table 1, the stretching mode with a PED value is 100 %. In FTIR, the bending assignments were observed at 1392 cm^{-1}, 1124 $cm^{-1}$and 1186 cm^{-1}, in FT-Raman it is observed at 1186 cm^{-1} and its corresponding theoretical values contributed 30 % and 16 % to total plan bending vibration by IR and Raman, respectively. Table 1, shows that scaled vibrations using the theoretical methods are agreed with experimental data.

Methyl group vibration

The methyl group vibrations commonly occur as stretching, deformation and vibration. There was generally a stretching of C—H of 3000–2900 cm^{-1}[3] for methyl groups. The compound 1C4EB has

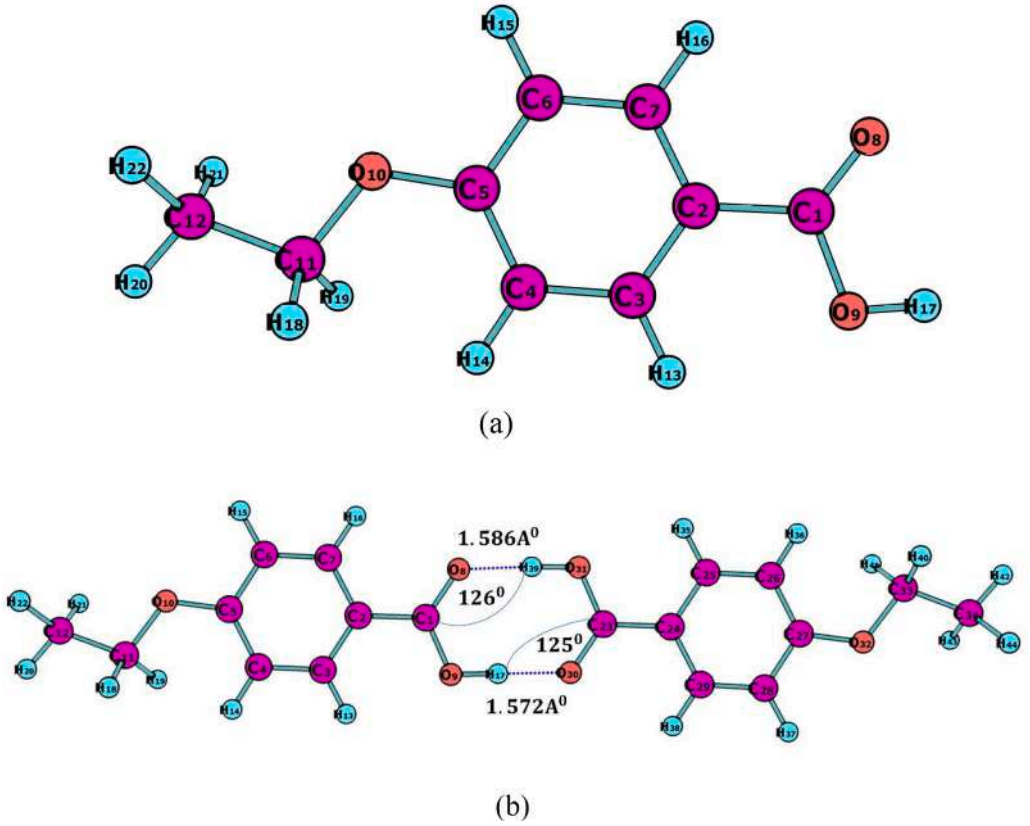

Fig. 1. Optimized structure of 1C4EB in (a) a monomeric space and (b) a dimeric space.

methyl and methylene groups, in the FTIR spectra the peaks observed at 2985 and 2944 cm^{-1} are ascribed to it respectively. The FT-Raman peaks at 2891 and 2869 cm^{-1} are attributed to methyl and methylene groups respectively. In PED, contributions range from 96 to 100 %. The C—H in-plane bending vibrations for IR and Raman are 1043 cm^{-1} and 1045 cm^{-1} by PED values of 26 and 12 %. The aromatic C—H vibration frequencies match the literature [4].

Carbon–Hydrogen vibrations

The stretching of C—H bonds usually occurs between 3100 and 3000 cm^{-1} [32]. The IR and Raman spectra showed phenolic C–H stretching bands appeared at 3083 cm^{-1} and 3072 cm^{-1} respectively. Theoretically, the C—H aromatic stretching bands appeared at 3078 and 3093 cm^{-1} by the HF method and at 3063 cm^{-1}, and 3078 cm^{-1} by the DFT technique with 99 % in PED and exhibited a strong concurrence. A strong and characteristic C—H bending vibration appeared between 1390 and 990 cm^{-1} [33]. In FTIR, the in-plane C—H bending vibrations are observed at 1321, 1300, 1115, and 1043 $cm^{-1}$and in Raman, the same in-plane bending peaks are observed at 1389, 1229 and 1038 cm^{-1} and PED percentages of 79 %, 63 %, 24 % and 26 % for the selected system and the C–H vibrations are well in agreement between theory and experiment.

Carbon–Carbon vibrations

The C—C stretching vibrations occurred between the range of 1200 - 1680 cm^{-1} [34,35]. The characteristics C—C stretching peaks appeared at 1678, 1607, 1430 and 1321 cm^{-1} in IR spectrum and observed at 1609, 1422 and 1320 cm^{-1} in FT-Raman. The theoretically calculated peaks at 1628, 1600, 1434 and 1316 cm^{-1} in FTIR and 1594, 1441 and 1352 cm^{-1} in Raman were found to have a PED assignment percentage of approximately 50 % [36]. The experimental and theoretical values demonstrate a significant level of agreement and Table 1 provides the vibrational modes of C—C vibrations.

Carbon–Oxygen vibrations

The C=O stretching band exhibits significant vibrational bands between 1870 and 1540 cm^{-1}. The FT-IR analysis found the C=O stretching peak of the C(=O) OH group of 1C4EB is at 1800 cm^{-1} [37]. The computed C=O stretching vibrations are assigned to the peaks that appeared at the 1788 and 1764 cm^{-1} band in FT-IR and FT-Raman spectra contributing 82 %. The absorption of the molecule under investigation was enhanced by elongating the C—O group. Vibrations associated with stretching of light substituents were observed between 1095 and 1310 cm^{-1}. The IR and Raman spectra of this molecule revealed weak C—O stretching vibrations. In the FT-Raman analysis, in-plane bending vibrations of C—O were identified at 628/629 cm^{-1} (PED-43 %) these vibrations appeared weak in the Raman analysis [38].

Natural bond orbital analysis

It is an effective technique to determine the bond order between two atoms and the electrical charge on each atom. Moreover, it employs the 2nd-order Fock Matrix was analyzed using second-order perturbation theory as reported in the literature [39,40] to investigate the interactions occurring within and between molecules involving the compound 1C4EB and values shown in table S2. It has been approximated that the energy stabilization $E_{(2)}$ arises from the electron delocalization between NBOs (i, j), which act as donors and acceptors. This was a result of the orbital imbricate among σ (C–C, C–H) and π (C–O); σ*(C–C, C–H) and π*(C–O) bond orbitals causing charge transfer (intramolecular) and stabilizing the system. Because of these interactions, the electron density in the C–C antibonding orbital increases, weakening their bonds [41]. Table S2 shows the intramolecular hyperconjugation interaction

Table 1
The FT-IR, FT-Raman assignments of 1C4EB.

Sym. species	Experimental		HF/6–311++*G*(d,p)		B3LYP/6–311++*G*(d,p)		Assignment PED
	FTIR	FT-Raman	unscaled	Scaled	unscaled	Scaled	
A′	3423		4127	3422	3776	3413	ν_{OH}(100)
A′	3083		3380	3078	3215	3093	ν_{CH}(99)
A′			3371	3069	3203	3082	ν_{CH}(98)
A′		3072	3363	3062	3201	3079	ν_{CH}(99)
A′			3352	3052	3189	3036	ν_{CH}(99)
A′	2985	2985	3253	2961	3115	2965	ν_{CH}(96)
A′	2942	2944	3239	2949	3106	2957	ν_{CH}(99)
A′	2891	2892	3205	2882	3042	2896	ν_{CH}(100)
A′			3176	2856	3039	2893	ν_{CH}(99)
A′	2824	2870	3166	2881	3004	2860	ν_{CH}(100)
A′	1800		1965	1788	1778	1764	ν_{OC}(82)
A′	1678		1789	1628	1647	1633	ν_{CC}(42)
A′	1607	1609	1750	1600	1607	1594	ν_{CC}(48)+β_{CCC}(22)
A′			1677	1533	1542	1530	β_{HCC}(23)+ β_{HCH} (13)
A′			1649	1507	1519	1507	β_{HCH}(75)
A″			1618	1479	1501	1489	β_{HCH}(53)+τ_{HCCO}(20)
A″			1600	1462	1485	1473	β_{HCH}(72)+ τ_{HCCO}(20)
A′	1430	1442	1569	1434	1452	1441	ν_{CC}(35)+ β_{HC}C(14)
A″			1559	1425	1427	1416	β_{HCH}(40)+ τ_{HCOC}(31)
A″			1521	1391	1402	1391	β_{HCH}(45)+ τ_{HCOC}(31)
A′	1392	1320	1491	1363	1363	1352	ν_{OC}(16)+ ν_{CC}(13)+ β_{HOC}(30)+ β_{OCO}(11)
A′	1321		1440	1316	1349	1339	ν_{CCC}(64)
A′	1321	1399	1421	1299	1328	1318	β_{HCC}(79)
A′	1300	1299	1414	1293	1305	1294	β_{HCC}(63)+ ν_{HCOC}(23)
A′	1261	1287	1330	1215	1280	1269	ν_{CC}(10)+ ν_{OC}(44)
A′	1124		1309	1196	1216	1206	ν_{CC}(23)+ β_{HOC}(30)+ β_{HCC}(27)
A′	1173	1186	1285	1175	1183	1173	β_{HOC}(16)+ β_{HCC}(40)
A″	1115	1138	1277	1168	1177	1120	β_{HCC}(24)+ τ_{HCOC}(24)
A″	1043		1238	1132	1140	1131	β_{HCC}(26)+ τ_{HCCO}(20)
A″	1043	1045	1204	1100	1134	1079	β_{HCC}(12)+ τ_{HCCO}(26)
A′			1198	1095	1094	1041	ν_{OC}(40)
A′			1158	1058	1058	1007	ν_{CC}(39)+ ν_{OC}(40)
A′			1110	1015	1024	975	β_{HCC}(10)+ β_{CCC}(63)
A″			1097	1003	993	945	τ_{HCCC}(76)
A″	922	922	1081	988	967	920	τ_{HCCC}(92)+ τ_{CCCC}(20)
A″	852	842	1006	920	936	891	ν_{CC}(26)+ ν_{OC}(18)+ τ_{HCCO}(20)
A″	832	824	955	873	864	822	τ_{HCCC}(39)+ σ_{OCOC}(10)+ σ_{OCCC}(18)
A″			919	840	840	800	τ_{HCCC}(21)+ τ_{HCOC}(22)
A′			895	818	831	791	ν_{CC}(34)+ ν_{OC}(10)+ β_{CCC}(11)
A″	772	774	892	815	819	779	τ_{HCCC}(52)
A″		763	871	796	783	745	τ_{HCCC}(10)+ σ_{OCOC}(54)
A′			804	735	739	704	ν_{OC}(13)+ ν_{CC}(10)+ β_{CCC}(14)
A″	646	640	775	708	709	675	τ_{HCCC}(11)+ τ_{CCCC}(56)+ σ_{OCOC}(21)
A′			693	633	646	615	β_{CCC}(54)
A′	628	629	678	619	626	621	β_{OCO}(43)+ β_{CCC}(14)
A″	553		605	553	567	540	τ_{HOCC}(76)
A′			551	504	509	485	β_{OCC}(46)+ β_{CCC}(14)
A″			547	500	505	481	τ_{HOCC}(14)+τ_{HCCC}(10)+ τ_{CCCC}(12)+ σ_{OCCC}(31)
A′			502	459	469	446	ν_{CC}(12)+ β_{OCO}(46)
A″	469		462	423	423	403	τ_{HCCC}(10)+τ_{CCCC}(37)
A′		318	423	387	396	377	β_{OCC}(40)+ β_{CCO}(33)
A″		257	318	290	289	275	τ_{CCCC}(13)+ σ_{CCCC}(36)+ σ_{OCCC}(15)
A″			302	276	284	270	ν_{OC}(11)+ ν_{CC}(14)+ β_{CCC}(14)+ β_{CCO}(20)
A″	257		274	250	253	241	τ_{HCCO}(83)
A′			235	215	219	208	β_{OCC}(38)+ β_{CCC}(40)
A′			134	122	124	118	β_{OCC}(69)+ β_{CCC}(22)
A″			133	121	122	116	τ_{CCCC}(33)+ τ_{CCOC}(16)+ σ_{CCCC}(30)
A″			113	103	108	103	τ_{CCOC}(16)+ τ_{COCC}(60)
A″			76	69	68	65	τ_{OCCC}(86)
A″			49	45	47	44	τ_{CCCC}(14)+ τ_{CCOC}(60)

ν-stretching,.
β-in plane bending,.
σ-out plane bending and.
τ-torsion.

between the π* (C_1–O_8) and the π* (C_2-C_3) bonds to stabilization of 66.15 kJ/mol respectively due to antibonding orbitals. The magnitude of charge transferred from ($LP_{(2)}$ O_{10}) → π* (C_4–H_5) and ($LP_{(1)}$ O_9) → π* (C_1–O_8) showed that stabilization energy of about ~24.88 kJ/mol and ~ 35.28 kJ/mol respectively. This results in electrons being transferred from donor i to acceptor j. As a result, anti-bonding atoms combine to form bonding atoms. The stabilization energies of a molecule can be used to verify charge transfer episodes.

Nonlinear optical properties

NLO features included optical modulation, memory, switching,

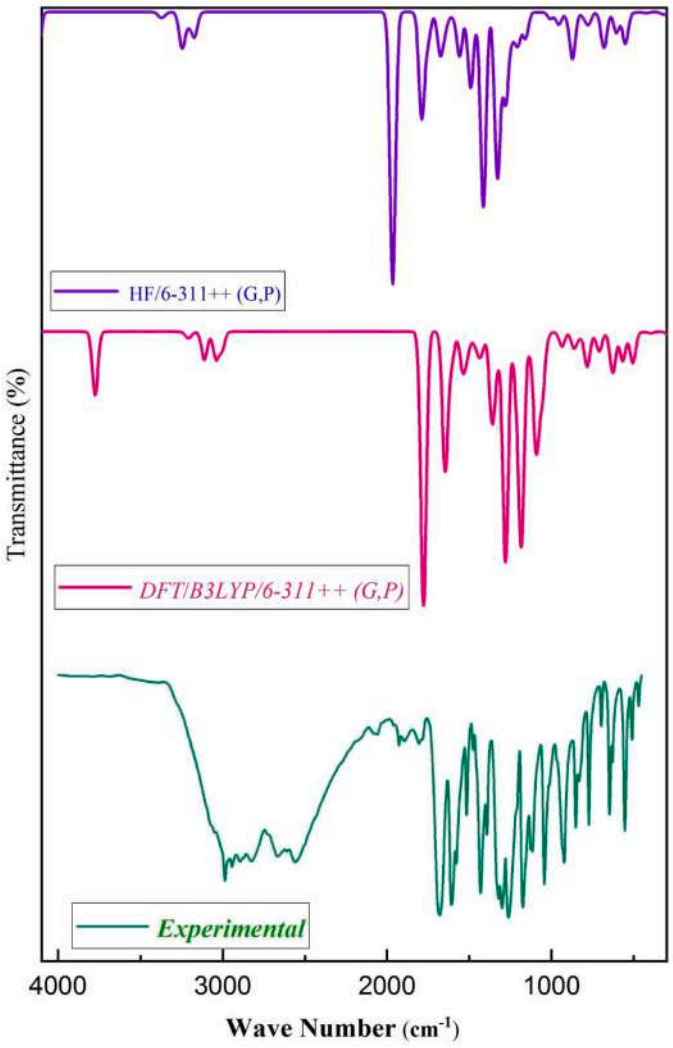

Fig. 2. Experimental and theoretical FT-IR spectra of *1C4EB*.

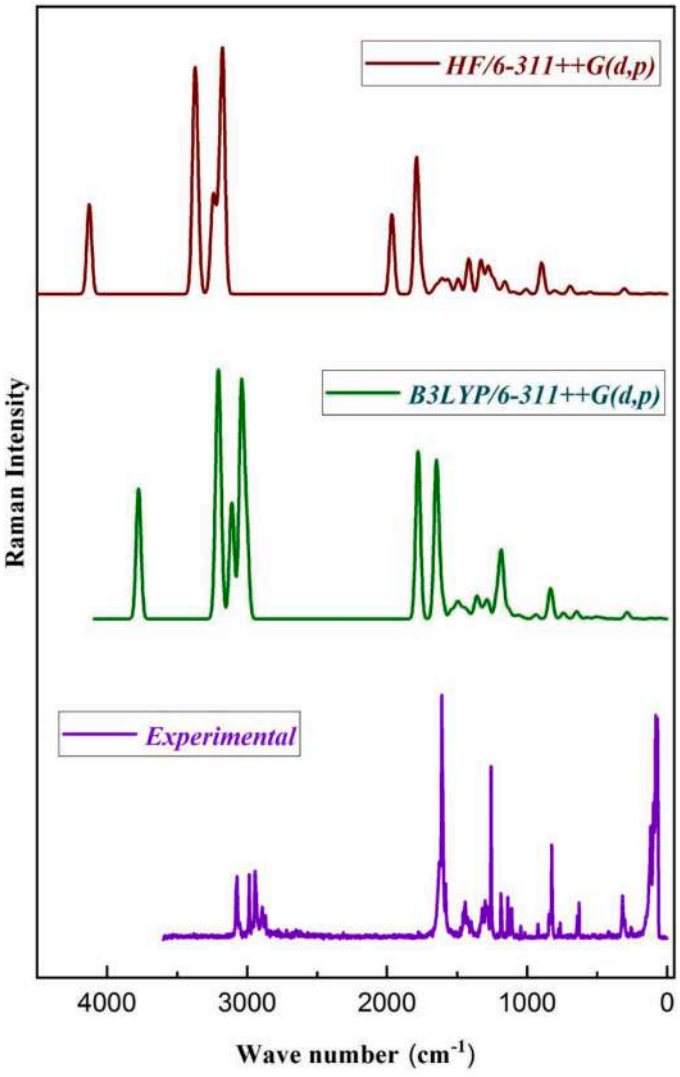

Fig. 3. Experimental and theoretical FT-Raman spectra of *1C4EB*.

frequency shifting and optical logic to improve optical signal processing, data storage and current communication technologies. Non-linear effects change the amplitude of a new electromagnetic field, frequency, or phase [42–45]. Table 2 presents the values of the NLO properties of 1C4EB. The first-order hyperpolarizability for this compound is measured at 7562.93×10^{-33} esu. In contrast, the corresponding value for urea is 372×10^{-33} esu. Additionally, the dipole moment value for the component μ_{total} is determined to be 1.2270 D, while the polarizability value is measured at 47.4847×10^{-24} esu. These values collectively indicate that the molecules comprising 1C4EB exhibit superior properties as an NLO material.

Table 2
The NLO properties of 1C4EB.

Parameters	Values	Parameters	Values
μ_x	−0.7576	β_{xxx}	8754.20
μ_y	−0.9652	β_{xxy}	504.07
μ_z	0.0065	β_{xyy}	−889.81
$\mu_{tot\ (D)}$	1.2270	β_{yyy}	−373.62
α_{xx}	26.2738	β_{xxz}	−58.13
α_{xy}	1.3806	β_{xyz}	−11.45
α_{yy}	17.7626	β_{yyz}	−0.4053
α_{xz}	−0.0628	β_{xzz}	−302.56
α_{yz}	0.0061	β_{yzz}	−236.63
α_{zz}	10.6374	β_{zzz}	−5.3021
$\alpha_{tot\ (esu)}$	18.2246×10^{-24}	$\beta_{tot\ (esu)}$	7562.93×10^{-33}
Δα (esu)	47.484710^{-24}		

Mulliken charges

The Vibrational properties of molecules are directly related to Mulliken charges. The present system 1C4EB, quantifies the effects of atomic displacement on the electronic structure of the molecules and associated with the chemical bonds present in the molecule. Several other properties of molecules including dipole moments and polarizability are also affected. Fig. 4 illustrates the bar chart of the charges of the individual atoms of 1C4EB. Table S3 presents the Mulliken charges obtained theoretically. The charge distribution of the current investigation showed all hydrogen atoms were positively charged and as expected all oxygen atoms were negative. A study found that the magnitude of 1C4EB's atomic charges on carbon atoms was both positive and negative [46].

The theoretical UV–Vis analysis

An analysis of the ultraviolet spectra of 1C4EB has been carried out in gas, water, DMSO, acetone and chloroform mediums using a theoretical approach. The low-lying excited states were obtained for the optimized ground state structure of 1C4EB by TD-DFT [47]. Table 3 provided absorption wavelengths, oscillatory strengths and theoretical

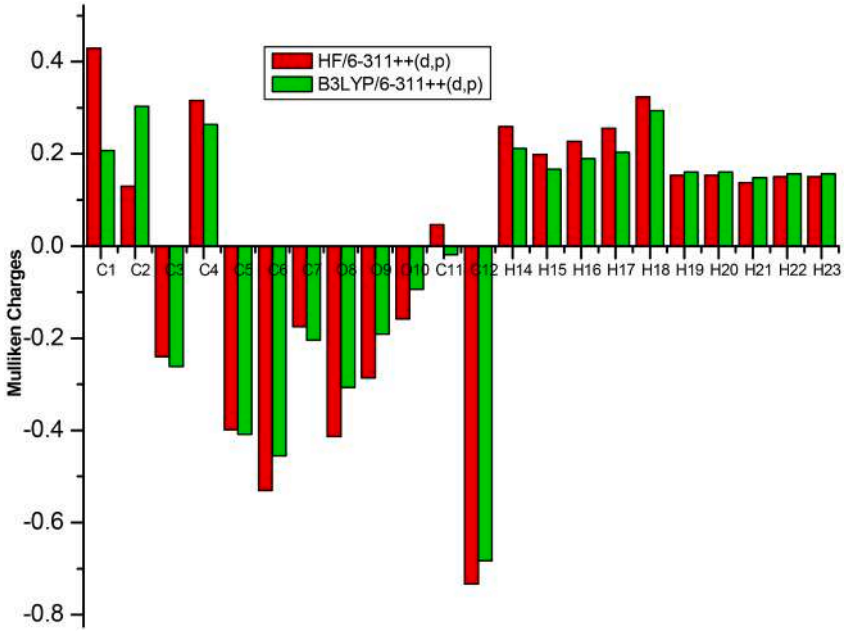

Fig. 4. Mulliken charge distribution of 1C4EB.

Table 3
The UV–Vis analysis of 1C4EB in gas and four different mediums.

Solvents	State	Assignment	Coefficient	Energy (eV)	Wave Length (nm)	Oscillator strength
Gas	S_0-S_1	H->LUMO	4.64 %	4.8789	254.12	0.4074
		H->LUMO +1	93.38 %			
	S_0-S_4	H->LUMO	96.32 %	5.5491	223.43	0.0071
	S_0-S_6	H->LUMO	97.24 %	5.8975	210.23	0.0007
Water	S_0-S_1	H->LUMO	97.70 %	4.5712	271.23	0.6837
	S_0-S_4	H->LUMO	2.79 %	5.5049	225.22	0.3500
		H->LUMO +1	50.81 %			
	S_0-S_6	H->LUMO	96.75 %	6.0798	203.93	0.0078
DMSO	S_0-S_1	H->LUMO	97.66 %	4.5755	270.97	0.6798
	S_0-S_4	H->LUMO	46.10 %	5.5098	225.03	0.3463
		H->LUMO +1	50.73 %			
	S_0-S_6	H->LUMO	96.84 %	6.0772	204.01	0.0076
Acetone	S_0-S_1	H->LUMO	97.56 %	4.589	270.18	0.6674
	S_0-S_4	H->LUMO	46.57 %	5.5248	224.42	0.3350
		H->LUMO +1	50.47 %			
	S_0-S_6	H->LUMO	97.11 %	6.0692	204.28	0.0070
Chloroform	S_0-S_1	H->LUMO	96.94 %	4.6606	2f66.03	0.6024
	S_0-S_4	H->LUMO	47.08 %	5.6021	221.32	0.2817
		H->LUMO +1	49.09 %			
	S_0-S_6	H->LUMO	98.08 %	6.0252	205.78	0.0045

electronic excitation energies. Fig. 5 shows the decreasing trend of theoretical wavelengths in the following order: Water (271.23 nm) > DMSO (270.97 nm) > Acetone (270.18 nm) > Chloroform (266.03 nm) > Gas (254.12 nm) with oscillator strength values of 0.6837, 0.6898, 0.6644, 0.6024 and 0.4074 for ground and first excited states, respectively. According to the calculations, 96–98 % of the HOMO-LUMO transitions have been assigned to the various solvents used, while 96 % has been assigned to the gaseous phase. Based on the observations, the compound has higher stability in polar solvents [48].

Quantum chemical properties and the HOMO-LUMO map

In HOMO and LUMO parameters, the Molecular Orbital is a significant chemical and biological feature. The HOMO donates electrons, while the LUMO gains electrons. The active mechanism of FMO can be gained from studies of this compound by physicists and chemists [49, 50]. FMO surface maps of different solvents and gas phases are shown in Fig. 6. Using the B3LYP basis set, the FMO was calculated using Gaussian software. Table 4 presents the calculated Conceptual DFT supported by global reactivity descriptors for the analysis in different solvents. An energy gap exists between the FMO of gas and polar solvents such as water, Acetone, DMSO and Chloroform of 5.1707, 5.0719, 5.0771, 5.0733 and 5.0978 eV respectively. There is a negative chemical potential for the compound, indicating that the compound is stable. The chemical hardness value indicates whether the molecule is hard or soft. High electrophilicity index values are attributed to the biological effect of the compound [51].

Thermodynamic properties

Table 5 lists the theoretical harmonic frequencies that have been calculated for the static thermodynamic properties: heat capacity ($C^0_{p,m}$), entropy (S^0_m) and enthalpy (ΔH^0_m) for the title molecule at a higher accurate level and determined by the Perl script. In Table 5, the molecular vibrational intensities increased with temperatures between 100 K and

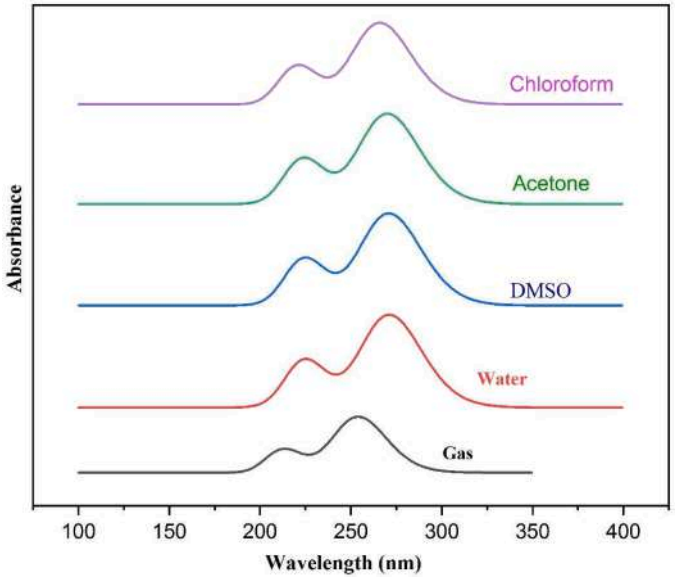

Fig. 5. The theoretical UV–Vis spectra of 1C4EB in gas and four different mediums.

1000 K, thereby increasing these thermodynamic functions. According to these thermodynamic properties, fitting factors (R^2) were 0.9995, 0.9999 and 0.9995, respectively. Fig. 7 shows the correlation graphics for the corresponding fitting equations. As a result, 1C4EB demonstrates its high thermal stability when exposed to high temperatures

$$C = 15.2337 + 0.5737\ T - 2.3915 \times 10^{-4}\ T^2\ \left(R^2 = 0.9995\right)$$

$$S = 229.9108 + 06515\ T - 1.588 \times 10^{-4}\ T^2\ \left(R^2 = 0.9999\right)$$

$$\Delta H = -6.4366 + 0.07571\ T - 1.5609\ \times 10^{-4}\ T^2\ \left(R^2 = 0.9995\right)$$

Molecular electrostatic potential surface (MEP) analysis

An extensive range of chemical systems has been analyzed using electrostatic potentials for predicting and interpreting their reactive behavior and intermolecular interactions. Multiwfn 3.8 and VMD 1.9.3 were used to calculate the Electrostatic Potential, illustrate electrostatic interactions among molecules and determine reactive sites [52–55]. Fig. 8(a) shows the Van der Waals surface and the extrema surface mapped using ESP. The Blue and golden spheres in Fig. 8(a) represent ESP surface local minimum and maximum points. A positive extrema in this area also indicates that nuclear charges dominate the electrostatic potential. Electrons contribute more to the negative extreme points [56]. A large negative value of O_8 in the carbonyl group (−41.62 kcal/mol) has to act as the lone pair of oxygen at the surface, resulting in the global minimum. The ESP at maximum (48.39 kcal/mol) is much larger than at other positive values due to the positively charged hydroxy group of H_{17}. Fig. 8(b) shows that, on average, 52 % of all surface areas correspond to ESP values between −10 and 19 kcal/mol, whereas about 43 % and 54.5 % of all surface areas correspond to ESP values in the positive and negative ranges, respectively.

Fukui functional analysis

Fukui's function describes an electron density after some electrons have been added or removed. It can determine the most electrophilic and nucleophilic active sites of 1C4EB were calculated by the DFT method and Multiwfn 3.8 program and the values are given in Table S4, Fukui functions are commonly expressed in the following way [57].

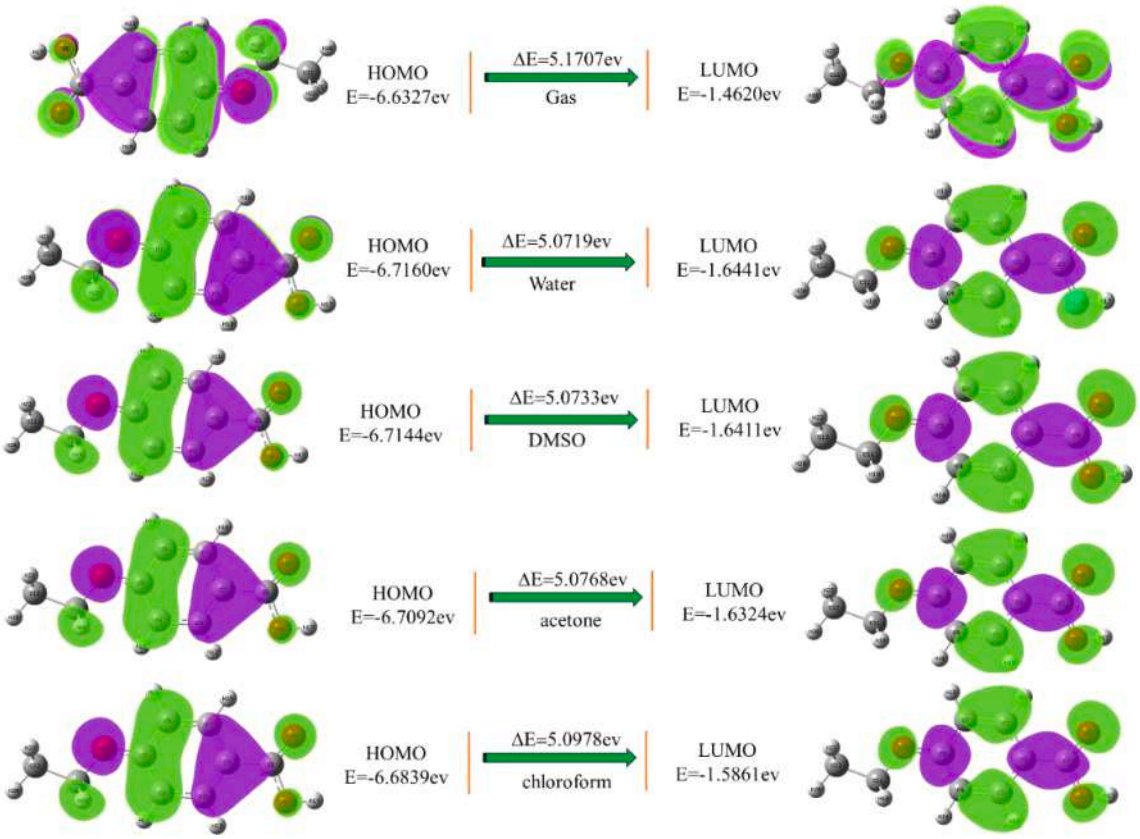

Fig. 6. HOMO & LUMO surface maps of the 1C4EB in gas and four different mediums.

Table 4
The FMO and GCRD values of 1C4BA.

Medium	Energy (in eV)			Global Chemical reactivity descriptor (in eV, except S (eV^{-1}))						
	HOMO	LUMO	ΔE	I	A	η	S	χ	μ	ω
Gas	−6.6327	−1.4620	5.1707	6.6327	1.4620	2.5854	0.1934	7.3637	−4.0474	3.1681
Water	−6.7160	−1.6441	5.0719	6.7160	1.6441	2.5360	0.1972	7.5381	−4.1801	3.4450
DMSO	−6.7144	−1.6411	5.0733	6.7144	1.6411	2.5367	0.1971	7.5350	−4.1778	3.4403
Acetone	−6.7092	−1.6321	5.0771	6.7092	1.6321	2.5385	0.1970	7.5253	−4.1707	3.4260
Chloroform	−6.6839	−1.5861	5.0978	6.6839	1.5861	2.5489	0.1962	7.4770	−4.1350	3.3540

Table 5
Thermodynamic properties of 1C4BA.

T (K)	$C^0_{p,m}$ (J mol^{-1} k^{-1})	S^0_m (J mol^{-1} k^{-1})	ΔH^0_m (KJ mol^{-1})
100	291.29	73.24	5.14
200	355.53	117.63	14.66
298	410.95	163.05	28.43
300	411.96	163.90	28.74
400	465.22	207.58	47.35
500	515.67	244.81	70.03
600	563.09	275.13	96.08
700	607.41	299.70	124.87
800	648.79	319.86	155.88
900	687.46	336.63	188.73
1000	723.60	350.70	223.12

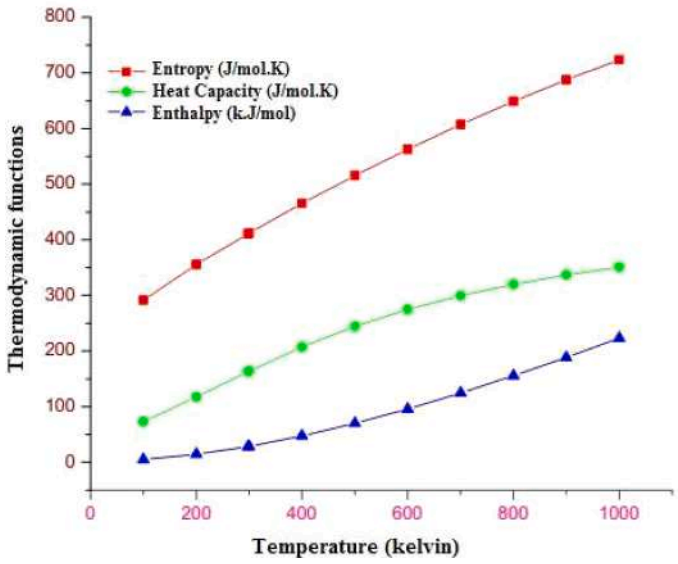

Fig. 7. Temperature Correlation graphic representations of 1C4EB.

$$f_\rho^- = \rho(N) - \rho(N-1)$$

$$f_\rho^+ = \rho(N+1) - \rho(N)$$

$$f_\rho^0 = \frac{1}{2}(\rho(N+1) - \rho(N-1))$$

$$\Delta f_\rho = \left(f_\rho^+ - f_\rho^-\right)$$

In Fig. 9, blue color regions indicate the vulnerable site of electrophile attacks and green regions indicate the vulnerable site of nucleophile attacks. In table S4, the negative values of Δf(r) indicate electrophilic attacked sites, whereas positive values of Δf(r) indicate nucleophilic attacked sites [50]. The 1C4EB molecule possesses ten electrophilic attacks and twelve nucleophilic attacks. Based on comparing these two types of attacks, it is evident that nucleophilic attacks are more reactive than electrophilic and radicals. The maximum electrophilic attack on 1C4EB molecules occurs at O_9 atoms and the maximum nucleophilic attack occurs at C_2 and O_{10} [58,59].

ELF and LOL analysis

The topological properties of the compound 1C4EB were performed by the Multiwfn 3.8 program. The Electron Localization function (ELF) and Localized orbital locator (LOL) are tools used for performing covalent bonding analysis, as they reveal regions of molecular space where the probability of finding an electron pair is high in a molecule 1C4EB. The ELF is a function of electron pair density; LOL is a function of overlying localized orbitals [60], both are similar chemical mappings due to their kinetic energy density dependence.

Fig. 10, shows the contour maps of the title compounds, ELF maps were built range of from zero to one. Especially the delocalized electrons are < 0.5. A LOL map range is > 0.5 may be reached when a dominant electron position governs the electron density [61]. Because of the existence of a nuclear layer or covalent bond, the electrons are strongly positioned in this place, as shown by the high value. It is found that the electron clouds in 1C4EB were delocalized among carbon atoms, as revealed in the blue-colored areas. The key points, their trajectories, chemical bonding and their relevant locations are indicated in red and orange portions of the ELF map in 1C4EB. These regions are located mostly around hydrogen atoms. In addition, ELF and LOL maps show that hydrogen atoms' central areas are in white. This means that the electron density was higher than the highest limit (i.e., 0.80) of the color scale [62].

IRI analysis

The IRI is valid for detecting covalent and hydrogen bonds, steric regions and halogen bonds. For 1C4EB, Fig. 11(a) shows the subsurface maps with IRI=1.0 and that IRI revealed the types of interactions including covalent bonds, steric repulsion between monomers and dimers, as well as the steric effect within each phenyl ring [63]. Furthermore, the Light-blue color indicates the existence of an H-bond between the hydroxyl and carbonyl group (ie., O—H…C=O group) in the dimer of 1C4EB. The IRI isosurface 0.75 shows a blue colour and a covalent link between carbon atoms. In addition, in Fig 11(b), the color-filled maps of IRI are plotted in the dimer plane for a better illustration of their different characteristics. This map clearly shows areas of stronger chemical bonds and weaker interactions indicated in Orange and Green colours in the map. Molecule structure and properties can be studied in greater detail with IRI analysis.

Molecular docking studies

An analysis of the 1C4EB molecule using the PASS [64] online server predicts the most active molecule to be a Sugar-Phosphatase inhibitor with a probability of 0.944 and the other active to be Arginine 2-monooxygenase inhibitor with a probability of 0.948. Based on the literature for sugar phosphatase inhibitors [65] and Arginine 2-monooxygenase inhibitors [66], we selected proteins 4UAR and 2EEP. The proteins were achieved from the RCSB protein data bank and their docking

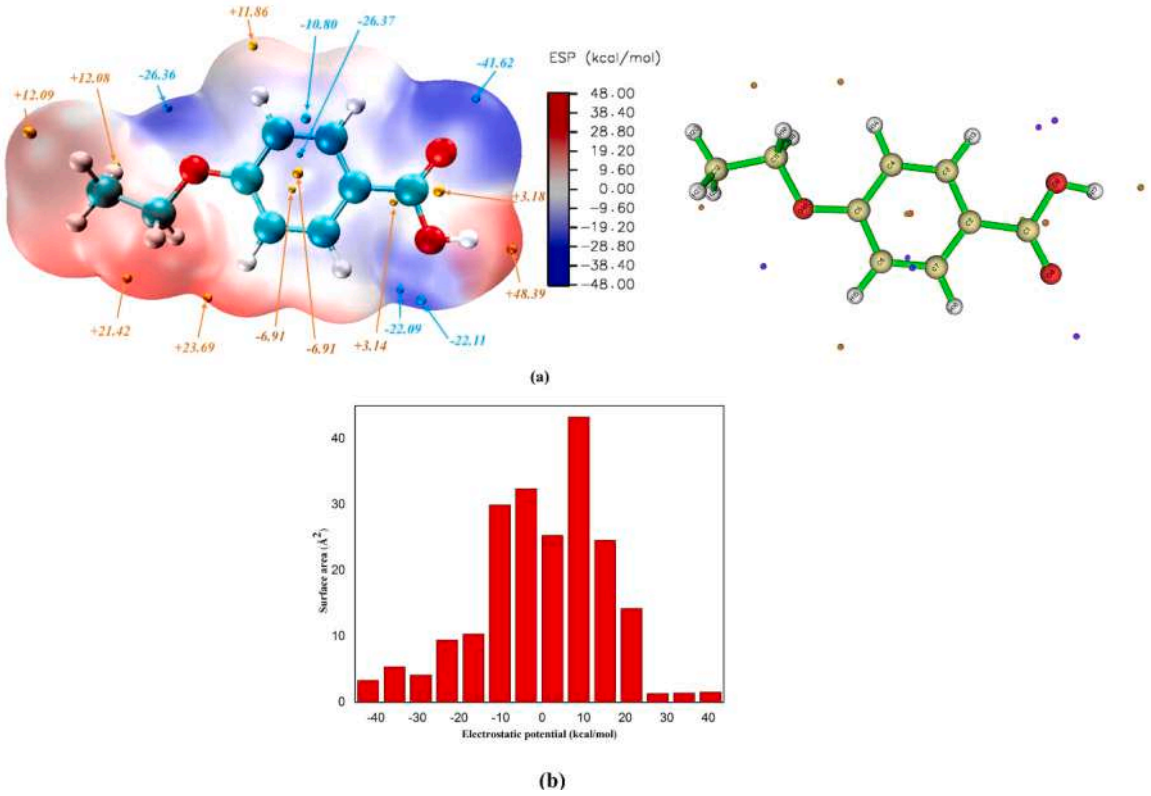

Fig. 8. (a) The ESP map with the surface local minima and Maxima as blue and gold spheres, and 8(b) System range of ESP surface area.

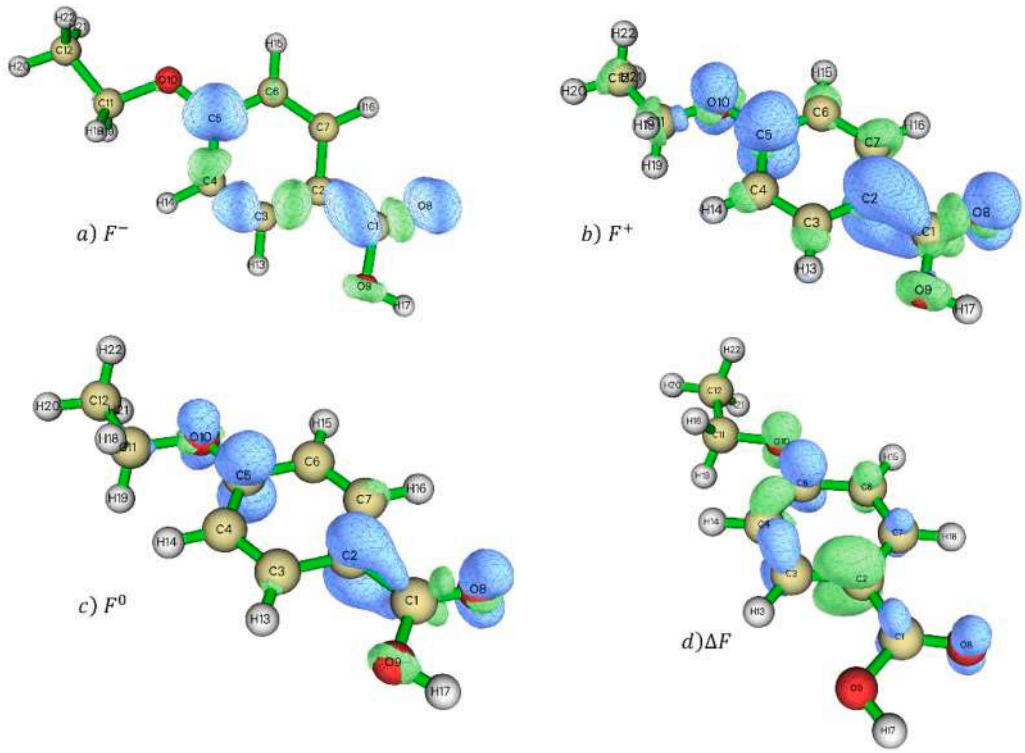

Fig. 9. The Fukui functions of 1C4EB.

analysis was performed by Auto Dock-Vina [67]. The PyMol system was used to visualize the implications of this calculation [68].

Fig. 12 shows Docking pocket, 3D and 2D views of the results of the molecular docked simulation for 4UAR and 2EEP proteins. Table 6 shows how different hydrogen bond residues interact with the protein and ligand and their bond distances. It has been determined that the pose with the lowest energy is the most suitable. As a result of these best poses, six hydrogen bonds were formed with neighboring hydrophobic

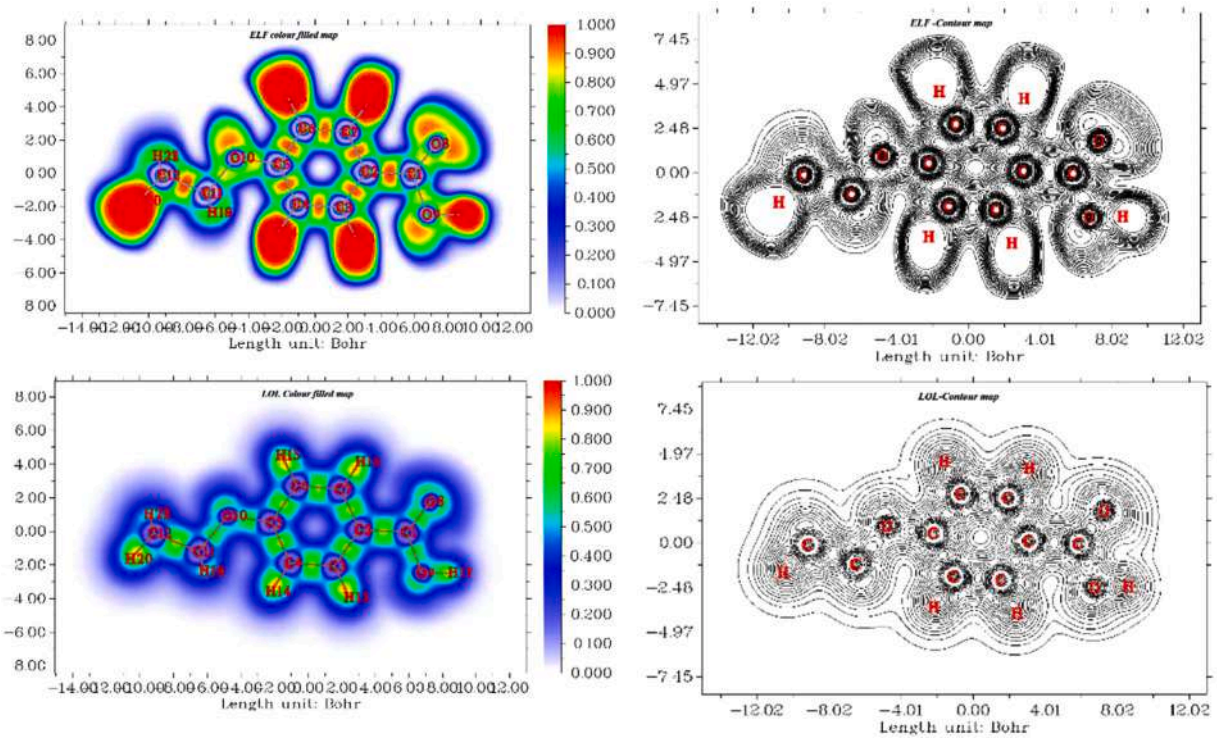

Fig. 10. ELF and LOL diagram of 1C4EB.

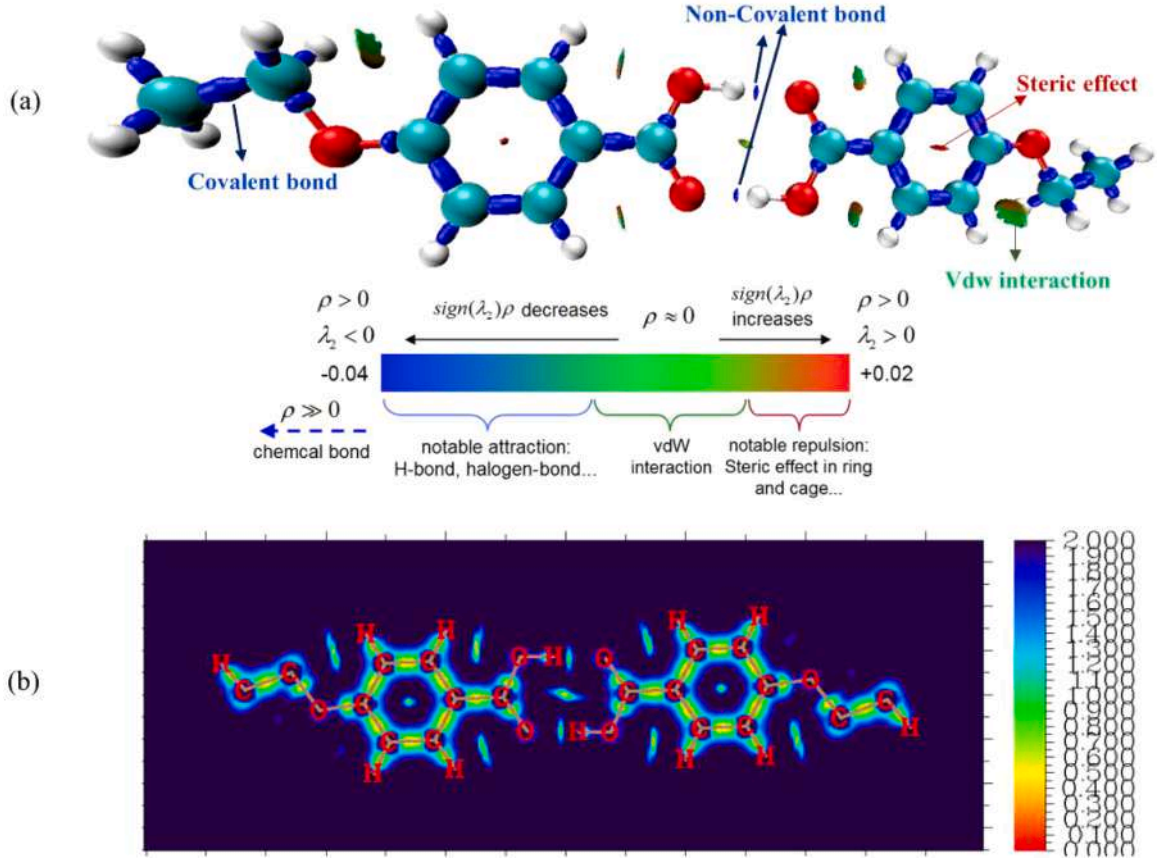

Fig. 11. a) IRI=1.0 isosurface Map b) IRI map on the dimer plane.

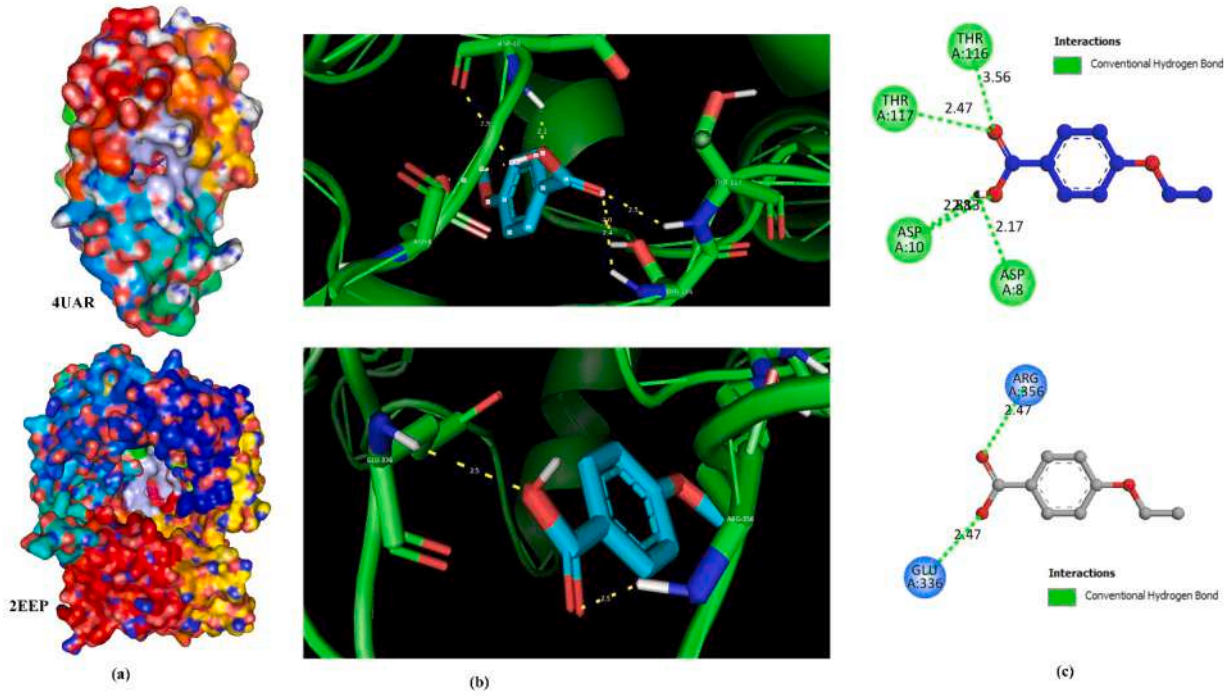

Fig. 12. Molecular docking of *1C4EB* (a) docking pocket (b) 3D view of protein and ligand interactions and (c) 2D view protein and ligand interactions with target Proteins 4UAR and 2EEP.

Table 6
Molecular docking results of 1C4EB with targeted proteins.

Proteins	No. of Hydrogen bonds	Bond Resides	Bond distance (Å)	Binding energy (kcal/mol)	Estimated Inhibition Constant (μm)
4UAR	6	THR-116	2.04	−6.7	12.20
		ASP-10	2.13		
		ASP-08	2.17		
		THR-116	2.43		
		THR-117	2.47		
		ASP-10	2.88		
2EEP	2	GLY-336	2.47	−4.7	358
		ARG-356	2.47		

residues with a free binding energy of −6.17 kcal/mol for 4UAR. The study of sugar phosphatase inhibitor activity was found to be three hydrogen bonds with target molecule (C3CA) [65], comparably the title molecule 1C4EB of the present study possess superior activity. Furthermore, 1C4EB binds to Arginine 2-monooxygenase inhibitor protein 2EEP by the binding score of −4.7 kcal/mol and two H-bonds. Therefore, 1C4EB can considered as a potent activator of sugar phosphatase due to its excellent affinity for targeted receptors, the effectiveness can be improved by further experiments.

Molecular dynamics simulation

After performing Molecular Dynamics simulations, Evaluations were carried out on several parameters, including RMSD, radius of gyration and intermolecular H- H-bonding. Using molecular dynamics simulations, a ligand-protein complex stability can be determined by RMSD and radius of gyration. Fig. 13 shows the results of a molecular dynamics simulation of 4UAR and 2EEP with the 1C4EB complex. As shown in Figs. 13a, 13b and 13d show that the 4UAR-1C4EB and 2EEP-1C4EB complexes remained stable during the MD simulation. The average RMSD of 4UAR was 0.128 nm, while that of 2EEP was 0.148 nm after the least square fitting to the backbone. The average protein Rg values were 1.7598 nm in 4UAR and 2.65 nm in 2EEP. In Fig. 13c, in the time domain, the 4UAR-2EEP position appears to have changed significantly around 0.026 ns and slightly around 0.065 ns. The equilibrium position of the ligand was reached at the 0.629 ns of the simulation and the position was maintained for the remainder of the simulation. The 4UAR-1C4EB complex was found to have an average RMSD of 0.0516 nm after the least squares fit protein. A least square fit to the protein (2EEP) increased in RMSD of the ligand until 0.115 ns. After the 0.422 ns of the MD simulation, it decreased gradually and reached equilibrium (Fig. 13a). The average RMSD of 2EEP-1C4EB after the least square fit to protein was 0.0569 nm [68]. As part of the MD simulation, the number of hydrogen bonds was also monitored (Fig. 13C). Results showed that at least one or three H-bonds are formed among the ligand and 4UAR in nearly one-third of the simulation time. One H-bond was formed between the ligand and 2EEP in nearly half of the simulation time [69].

MM-PBSA estimation

The MM-PBSA estimation was utilized for 4UAR and 2EEP in 1C4EB complexes to find the free binding energy. Table 7 lists the calculated energies of the non-bonded interactions were calculated for both complexes. The simulation was performed for 1 ns by using the MM-PBSA method, the binding free energy of −16.04 kJ/mol and −14.81 k mol^{-1} were calculated for complexes 1C4EB with 4UAR and 2EEP and the 1C4EB compounds. The energies exhibited a favorable interaction with the target proteins, as evidenced by the negative values of the ΔG binding energy. From the table 7, the complexes 4UAR and 2EEP with 1C4EB were found to have electrostatic energy averages (ΔE_{elec}) of −2.58 and −3.34 kJ mol^{-1}, respectively and Van der Waal energies of −28.56 and −25.24 kJ mol^{-1}. For the 4UAR and 2EEP, the average ΔG Polar values were 17.18 and 13.78 kJ mol-1, respectively. The corresponding computed values for ΔG non-Polar were −42.14 and −28.59

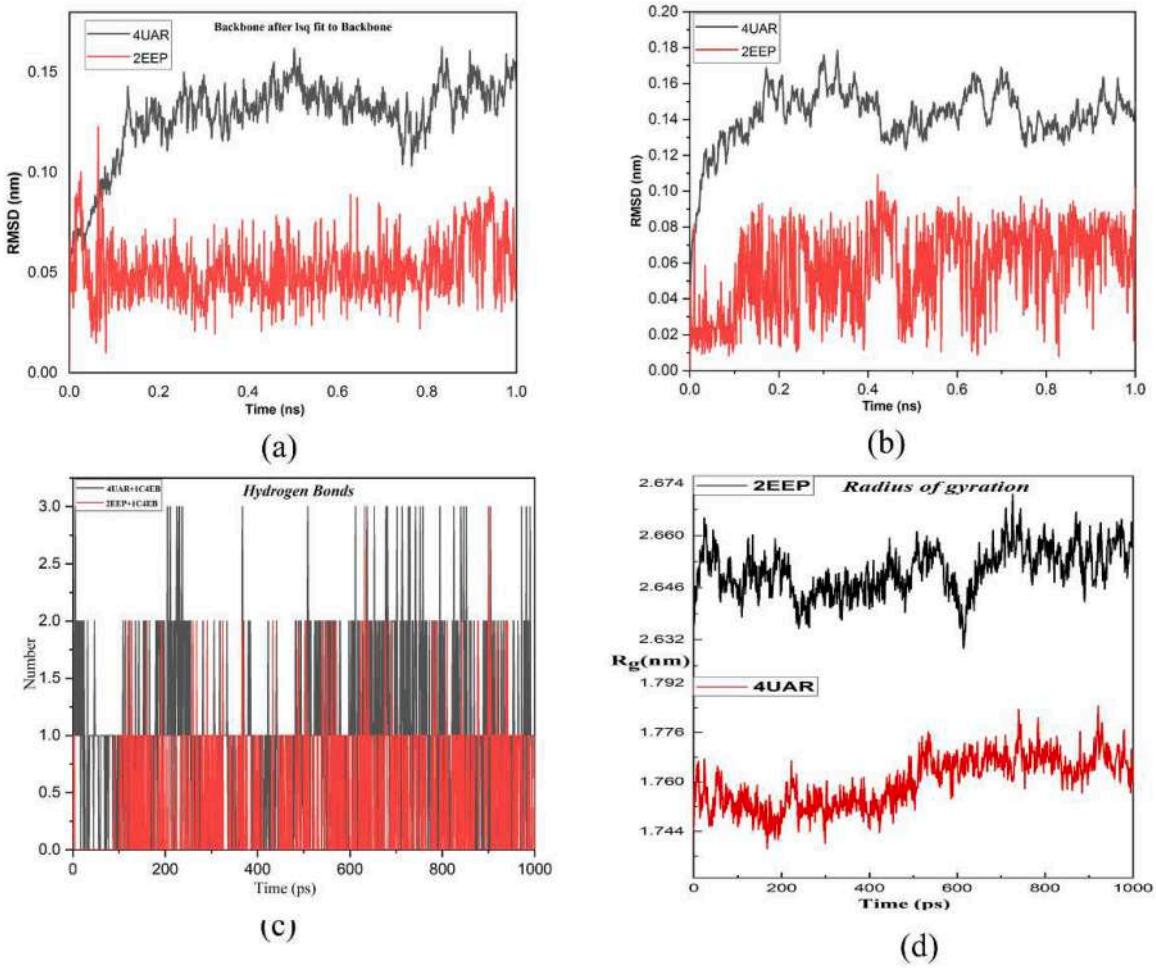

Fig. 13. MD simulation results (a) RMSD of backbone, (b) RMSD of ligand after least square fit to protein (c) number of hydrogen bonds between proteins (black-4UAR, Red-2EEP) and (d) Radius of gyration of proteins.

Table 7
Binding free energy for 1C4EB with 4UAR and 2EEP by MM-PBSA method.

Energy (in KJ/mol)	4UAR-1C4EB	2EEP-1C4EB
Van der Waal energy (ΔE_{vdW})	−28.56	−25.24
Electrostatic energy (ΔE_{elec})	−2.58	−3.34
Polar solvation energy (ΔG_{polar})	17.18	13.78
Non-polar solvation energy ($\Delta G_{non\ polar}$)	−42.14	−28.59
ΔG_{bind}	−16.04	−14.81

kJ mol^{-1}[70-71].

Conclusions

The study discussed the experimental and theoretical vibrational assignment of 1C4EB using HF and DFT methods. By NBO analysis, the magnitude of intramolecular charge transfer between bondings and the stabilization of 1C4EB. The high stabilization energy in this analysis was 66.15 kJ/mol. The values of first-order hyperpolarizability, polarizability and dipole moment is found to be 7562.93×10^{-33} esu, 47.4847×10^{-24} esu and 1.2270 D respectively, the values collectively exhibit superior properties as an NLO material. UV/Vis analyses for gas and different solvents were done using TD-DFT reveals that the wavelength of 1C4EB in gas is 254.12 nm and for solvents are 271.23 nm (Water), 270.97 nm (DMSO), 270.18 nm (Acetone), 266.03 nm (Chloroform) it indicating that solvent phase displays good activity and the similar trend observed for the oscillator strength describing the changeover the energies among the different atom or molecule. HOMO & LUMO energy gap is lesser in solvents in comparison with gas mediums, lower energy band gap indicating that the compound is chemically stable and good candidate for biological purposes. The thermodynamics properties correlation increased molecular vibration intensities ensuing increased heat capacities, entropies and enthalpies. The Fukui functional analysis exposes that the 1C4EB molecules are attacked by ten electrophiles and twelve nucleophiles. In ESP-mapped Van der Waals and extreme surfaces, nuclear charges dominate electrostatic potential. ESP values are −20 to 20 kcal/mol, with C—H hydrogens contributing the most. Multi-wave functional analyses explain bondings within a molecule. IRI can detect chemical bonds, hydrogen, steric and halogen bonds. Strong and weak interactions are evident from IRI isosurface maps. Docking studies revealed that 1C4EB molecules bind to sugar phosphatase inhibitor and Arginine 2-monooxygenase inhibitors proteins with affinities of −6.17 kcal/mol and −4.7 kcal/mol respectively. Based on these results, title molecules may adversely affect the 4UAR protein. MD revealed the steadiness of docked 4UAR and 2EEP structures in the active site of 1C4EB with considerable binding free energies of −16.04 and −14.81 kJ/mol.

Research data

All related research data are incorporated in manuscript and Table file.

CRediT authorship contribution statement

C.P. Devipriya: Data curation, Visualization, Software, Validation, Formal analysis, Resources. **S. Deepa:** Investigation, Writing – original draft, Writing – review & editing. **J. Udayaseelan:** Formal analysis, Resources. **RaviKumar Chandrasekaran:** Data curation, Visualization, Software, Validation, Formal analysis, Resources. **M. Aravinthraj:** Conceptualization, Methodology, Software, Validation, Supervision, Investigation, Writing – original draft, Writing – review & editing. **V. Sabari:** Investigation, Writing – original draft, Writing – review & editing.

Declaration of competing interest

The authors declare that they have no known competing financial interests or personal relationships that could have appeared to influence the work reported in this paper.

Data availability

No data was used for the research described in the article.

Supplementary materials

Supplementary material associated with this article can be found, in the online version, at doi:10.1016/j.chphi.2024.100495.

References

[1] M.A Palafox, J.L. Nunez, M. Gil, Theoretical quantum chemical study of benzoic acid: geometrical parameters and vibrational wavenumbers, Int. J. Quantum. Chem. 89 (1) (2002) 1–24, https://doi.org/10.1002/qua.10202.

[2] M.H Rahuman, S. Muthu, B.R. Raajaraman, M. Raja, H. Umamahesvari, Investigations on 2-(4-cyanophenylamino) acetic acid by FT-IR, FT-Raman, NMR and UV–Vis spectroscopy, DFT (NBO, HOMO-LUMO, MEP and Fukui function) and molecular docking studies, Heliyon 6 (9) (2020), https://doi.org/10.1016/j.heliyon.2020.e04976.

[3] S. Muthu, E. Isac Paulraj, Spectroscopic and molecular structure (monomeric and dimeric structure) investigation of 2-[(2-hydroxyphenyl) carbonyloxy] benzoic acid by DFT method: a combined experimental and theoretical study, J. Mol. Struct. 1038 (2013) 145–162, https://doi.org/10.1016/j.molstruc.2013.01.043.

[4] M. Cinar, N. Yildiz, M. Karabacak, M. Kurt, Determination of structural, spectrometric and nonlinear optical features of 2-(4-hydroxyphenylazo) benzoic acid by experimental techniques and quantum chemical calculations, Spectrochim. Acta Part A: Mol. Biomol. Spectrosc. 105 (2013) 80–87, https://doi.org/10.1016/j.saa.2012.12.009.

[5] M. Karabacak, Z. Cinar, M. Kurt, S. Sudha, N. Sundaraganesan, FT-IR, FT-Raman, NMR and UV–vis spectra, vibrational assignments and DFT calculations of 4-butyl benzoic acid, Spectrochim. Acta Part A: Mol. Biomol. Spectrosc. 85 (1) (2012) 179–189, https://doi.org/10.1016/j.saa.2011.09.058.

[6] M. Karabacak, M. Cinar, FT-IR, FT-Raman, UV spectra and DFT calculations on monomeric and dimeric structure of 2-amino-5-bromobenzoic acid, Spectrochim. Acta Part A: Mol. Biomol. Spectrosc. 86 (2012) 590–599, https://doi.org/10.1016/j.saa.2011.11.022.

[7] M. Karabacak, L. Sinha, O. Prasad, Z. Cinar, M. Cinar, The spectroscopic (FT-Raman, FT-IR, UV and NMR), molecular electrostatic potential, polarizability and hyperpolarizability, NBO and HOMO–LUMO analysis of monomeric and dimeric structures of 4-chloro-3, 5-dinitrobenzoic acid, Spectrochim. Acta Part A: Mol. Biomol. Spectrosc. 93 (2012) 33–46, https://doi.org/10.1016/j.saa.2012.02.110.

[8] A. Poiyamozhi, N. Sundaraganesan, M. Karabacak, O. Tanrıverdi, M. Kurt, The spectroscopic (FTIR, FT-Raman, UV and NMR), first-order hyperpolarizability and HOMO–LUMO analysis of 4-amino-5-chloro-2-methoxybenzoic acid, J. Mol. Struct. 1024 (2012) 1–12, https://doi.org/10.1016/j.molstruc.2012.05.008.

[9] M. Karabacak, L. Sinha, O. Prasad, AM. Asiri, M. Cinar, VK. Shukla, FT-IR, FT-Raman, NMR, UV and quantum chemical studies on monomeric and dimeric conformations of 3, 5-dimethyl-4-methoxybenzoic acid, Spectrochim. Acta Part A: Mol. Biomol. Spectrosc. 123 (2014) 352–362, https://doi.org/10.1016/j.saa.2013.12.015.

[10] M. Ramalingam, N. Sundaraganesan, H. Saleem, J. Swaminathan, Experimental (FTIR and FT-Raman) and ab initio and DFT study of vibrational frequencies of 5-amino-2-nitrobenzoic acid, Spectrochim. Acta Part A: Mol. Biomol. Spectrosc. 71 (1) (2008) 23–30, https://doi.org/10.1016/j.saa.2007.11.016.

[11] V.K. Rastogi, M.P. Rajpoot, S.N. Sharma, Infrared absorption spectra of some substituted benzoic, Indian J. Phys. 58 (4) (1984) 311–314.

[12] M.C. Gamberini, Y. Shyma Mary, Y. Sheena Mary, M. Krátký, J. Vinsova, C. Baraldi, Spectroscopic investigations, concentration-dependent SERS, and molecular docking studies of a benzoic acid derivative, Spectrochim. Acta Part A: Mol. Biomol. Spectrosc. 248 (2021) 119265, https://doi.org/10.1016/j.saa.2020.119265.

[13] R. Froissart, M. Piraud, A.M. Boudjemline, C. Vianey-Saban, F. Petit, A. Hubert-Buron, P.T. Eberschweiler, V. Gajdos, P. Labrune, Glucose-6-phosphatase deficiency, Orphanet. J. Rare Dis. 6 (2011) 27–39, https://doi.org/10.1186/1750-1172-6-27.

[14] J.P. Rake, G. Visser, P. Labrune, J.V. Leonard, K. Ullrich, G.P. Smit, Glycogen storage disease type I: diagnosis, management, clinical course and outcome. Results of the European Study on Glycogen Storage Disease Type I (ESGSD I), Eur. J. Pediatr. 161 (Suppl 1) (2002) S20–S34, https://doi.org/10.1007/s00431-002-0999-4.

[15] M.J. Frisch, G.W. Trucks, H.B. Schlegel, G.E. Scuseria, M.A. Robb, J.R. Cheeseman, G. Scalmani, V. Barone, B. Mennucci, G.A. Petersson, H. Nakatsuji, M. Caricato, X. Li, H.P. Hratchian, A.F. Izmaylov, J. Bloino, G. Zheng, J.L. Sonnenberg, M. Hada, M. Ehara, K. Toyota, R. Fukuda, J. Hasegawa, M. Ishida, T. Nakajima, Y. Honda, O. Kitao, H. Nakai, T. Vreven, J.A. Montgomery Jr., J.E. Peralta, F. Ogliaro, M. Bearpark, J.J. Heyd, E. Brothers, K.N. Kudin, V.N. Staroverov, T. Keith, R. Kobayashi, J. Normand, K. Raghavachari, A. Rendell, J.C. Burant, S.S. Iyengar, J. Tomasi, M. Cossi, N. Rega, J.M. Millam, M. Klene, J.E. Knox, J.B. Cross, V. Bakken, C. Adamo, J. Jaramillo, R. Gomperts, R.E. Stratmann, O. Yazyev, A. J. Austin, R. Cammi, C. Pomelli, J.W. Ochterski, R.L. Martin, K. Morokuma, V. G. Zakrzewski, G.A. Voth, P. Salvador, J.J. Dannenberg, S. Dapprich, A.D. Daniels, O. Farkas, J.B. Foresman, J.V. Ortiz, J. Cioslowski, D.J. Fox, Gaussian 09, Revision B.01, Gaussian, Inc., Wallingford CT, 2010.

[16] AD. Becke, Density-functional thermochemistry. I. The effect of the exchange-only gradient correction, J. Chem. Phys. 96 (3) (1992) 2155–2160, https://doi.org/10.1063/1.464913.

[17] W. Emori, H. Louis, SA. Adalikwu, RA. Timothy, C-Ru Cheng, TE. Gber, EC. Agwamba, AE. Owen, L. Ling, OE. Offiong, AS. Adeyinka, Molecular modeling of the spectroscopic, structural, and bioactive potential of tetrahydropalmatine: insight from experimental and theoretical approach, Polycycl. Aromat. Compd. 43 (7) (2023) 5958–5975, https://doi.org/10.1080/10406638.2022.2110908.

[18] DC. Young, A practical guide for applying techniques to real-world problems, Computat. Chem. 9 (2001) 390. New YorkISBN: 978-0-471-45843-2.

[19] B.N. Sundaraganesan, S. Ilakiamani, H. Saleem, PM. Wojciechowski, D. Michalska, FT-Raman and FT-IR spectra, vibrational assignments and density functional studies of 5-bromo-2-nitropyridine, Spectrochim. Acta Part A: Mol. Biomol. Spectrosc. 61 (13–14) (2005) 2995–3001, https://doi.org/10.1016/j.saa.2004.11.016.

[20] Jamroz, MH. "Vibrational energy distribution analysis VEDA 4." (2004).

[21] R. Dennington, T. Keith, J. Millam, GaussView, Semichem Inc., Shawnee Mission, KS, 2009.

[22] E.D. Glendening, A.E. Reed, J.E. Carpenter and F. Weinhold, NBO manual version 3.1, p 1–146.

[23] X.-H. Li, R.-Z. Zhang, X.-Z. Zhang, Natural bond orbital analysis of some para-substituted N-nitrosoacetanilide biological molecules, Struct. Chem. 20 (2009) 1049–1054, https://doi.org/10.1007/s11224-009-9508-y.

[24] J. Chocholoušová, V. Špirko, P. Hobza, First local minimum of the formic acid dimer exhibits simultaneously red-shifted O–H··· O and improper blue-shifted C–H··· O hydrogen bonds, Phys. Chem. Chem. Phys. 6 (1) (2004) 37–41, https://doi.org/10.1039/B314148A.

[25] AE. Reed, LA. Curtiss, F. Weinhold, Intermolecular interactions from a natural bond orbital, donor-acceptor viewpoint, Chem. Rev. 88 (6) (1988) 899–926, https://doi.org/10.1021/cr00088a005.

[26] T. Lu, F. Chen, Multiwfn: a multifunctional wavefunction analyzer, J. Comput., Chem. 33 (2012), https://doi.org/10.1002/jcc.22885.

[27] W. Lindstrom, et al., Using AutoDock for virtual screening, La Jolla (2008).

[28] Biovia, D.S., Discovery studio visualizer, v20.1.0.19295, (2016).

[29] Y. Tabuchi, K. Gotoh, H. Ishida, Crystal structures of three co-crystals of 4, 4′-bipyridyl with 4-alkoxybenzoic acids: 4-ethoxybenzoic acid–4, 4′-bipyridyl (2/1), 4-n-propoxybenzoic acid–4, 4′-bipyridyl (2/1) and 4-n-butoxybenzoic acid–4, 4′-bipyridyl (2/1), Acta Crystallogr. Sect. E: Crystallogr. Commun. 71 (11) (2015) 1290–1295, https://doi.org/10.1107/S2056989015018435.

[30] M. Aravinthraj, F. Liakath Ali Khan, J. Udayaseelan, A.A Fernandes, Dielectric relaxation and FTIR analysis of 2-chlorobenzoic acid with aniline and n-methyl aniline in 1, 4-dioxane, Mater. Today: Proceedings 47 (2021) 4391–4395, https://doi.org/10.1016/j.matpr.2021.05.201.

[31] D. Sajan, H. Joe, V.S. Jayakumar, J. Zaleski, Structural and electronic contributions to hyperpolarizability in methyl p-hydroxy benzoate, J. Mol. Struct. 785 (1–3) (2006) 43–53, https://doi.org/10.1016/j.molstruc.2005.09.041.

[32] N. Sundaraganesan, C. Meganathan, M. Kurt, Molecular structure and vibrational spectra of 2-amino-5-methyl pyridine and 2-amino-6-methyl pyridine by density functional methods, J. Mol. Struct. 891 (1–3) (2008) 284–291, https://doi.org/10.1016/j.molstruc.2008.03.051.

[33] A. Saral, R. Shahidha, M. Thirunavukkarasu, S. Muthu, Molecular structure, spectral, computational, IEFPCM investigation, and topological study on the biologically potent; cardiotonic drug 2-chloroquinolin-3-amine with structural optimization, Chem. Phys. Impact 6 (2023) 100193, https://doi.org/10.1016/j.chphi.2023.100193.

[34] M. Govindarajan, K. Ganasan, S. Periandy, M. Karabacak, S. Mohan, Vibrational spectroscopic analysis of 2-chlorotoluene and 2-bromotoluene: a combined experimental and theoretical study, Spectrochim. Acta Part A: Mol. Biomol. Spectrosc. 77 (5) (2010) 1005–1013, https://doi.org/10.1016/j.saa.2010.08.038.

[35] M. Karabacak, C. Karaca, A. Atac, M. Eskici, A. Karanfil, E. Kose, Synthesis, analysis of spectroscopic and nonlinear optical properties of the novel compound: (S)-N-

benzyl-1-phenyl-5-(thiophen-3-yl)-4-pentyn-2-amine, Spectrochim. Acta Part A: Mol. Biomol. Spectrosc. 97 (2012) 556–567, https://doi.org/10.1016/j.saa.2012.05.087.
[36] M. Karabacak, C. Karaca, A. Atac, M. Eskici, A. Karanfil, E. Kose, Synthesis, analysis of spectroscopic and nonlinear optical properties of the novel compound: (S)-N-benzyl-1-phenyl-5-(thiophen-3-yl)-4-pentyn-2-amine, Spectrochim. Acta Part A: Mol. Biomol. Spectrosc. 97 (2012) 556–567, https://doi.org/10.1016/j.matpr.2020.01.202.
[37] A.J. Barnes, M.A. Majid, M.A. Stuckey, P. Gregory, C.V. Stead, The resonance Raman spectra of Orange II and Para Red: molecular structure and vibrational assignment, Spectrochim. Acta a 41 (4) (1985) 629–635, https://doi.org/10.1016/0584-8539(85)80050-7.
[38] P. Rajkumar, S. Selvaraj, P. Anthoniammal, A. Ram Kumar, K. Kasthuri, S. Kumaresan, Structural (monomer and dimer), spectroscopic (FT-IR, FT-Raman, UV–Vis and NMR) and solvent effect (polar and nonpolar) studies of 2methoxy-4-vinyl phenol, Chem. Phys. Impact 7 (2023) 100257, https://doi.org/10.1016/j.chphi.2023.100257.
[39] P.S. Kalsi, Spectroscopy of organic compounds, New Age Int. (2007).
[40] C. James, A. Amal Raj, R. Reghunathan, I.H. Joe, V.S. Jayakumar, Structural conformation and vibrational spectroscopic studies of 2,6-bis(p-N,N-dimethyl benzylidene)cyclohexanone using density functional theory, J. RamanSpectrosc. 37 (2006) 1381–1392, https://doi.org/10.1002/jrs.1554.
[41] E.A. Adindu, O.C. Godfrey, E.I. Agwupuye, B.O. Ekpong, D.C. Agurokpon, S. E. Ogbodo, I. Benjamin, H. Louis, Structural analysis, reactivity descriptors (HOMO-LUMO, ELF, NBO), effect of polar (DMSO, EtOH, H2O) solvation, and libido-enhancing potential of resveratrol by molecular docking, Chem. Phys. Impact 7 (2023) 100296, https://doi.org/10.1016/j.chphi.2023.100296.
[42] H. Sekino, R.J. Bartlett, Hyperpolarizabilities of the hydrogen fluoride molecule: a discrepancy between theory and experiment? J. Chem. Phys 84 (1986) 2726–2733, https://doi.org/10.1063/1.450348.
[43] AE. Owen, H. Louis, EC. Agwamba, AD. Udoikono, A.-L.E. Manicum, Antihypotensive potency of *p*-synephrine: spectral analysis, molecular properties and molecular docking investigation, J. Mol. Struct. 1273 (2023) 134233, https://doi.org/10.1016/j.molstruc.2022.134233.
[44] VM. Geskin, C. Lambert, J.-L. Brédas, Origin of high second-and third-order nonlinear optical response in ammonio/borato diphenylpolyene zwitterions: the remarkable role of polarized aromatic groups, J. Am. Chem. Soc. 125 (50) (2003) 15651–15658, https://doi.org/10.1021/ja035862p.
[45] M. Nakano, H. Fujita, M. Takahata, K. Yamaguchi, Theoretical study on second hyperpolarizabilities of phenylacetylene dendrimer: toward an understanding of structure−property relation in NLO responses of fractal antenna dendrimers, J. Am. Chem. Soc. 124 (32) (2002) 9648–9655, https://doi.org/10.1021/ja0115969.
[46] S. Kanchana, T. Kaviya, P. Rajkumar, M. Dhinesh Kumar, N. Elangovan, S. Sowrirajan, Computational investigation of solvent interaction (TD-DFT, MEP, HOMO-LUMO), wavefunction studies and molecular docking studies of 3-(1-(3-(5-((1-methylpiperidin-4-yl) methoxy) pyrimidin-2-yl) benzyl)-6-oxo-1, 6-dihydro-pyridazin-3-yl) benzonitrile, Chem. Phys. Impact 7 (2023) 100263, https://doi.org/10.1016/j.chphi.2023.100263.
[47] G. Zhang, CB. Musgrave, Comparison of DFT methods for molecular orbital eigenvalue calculations, J. Phys. Chem. A 111 (2007) 1554–1561, https://doi.org/10.1021/jp061633o.
[48] J.K. Ojha, G. Ramesh, B.V. Reddy, Structure, chemical reactivity, NBO, MEP analysis and thermodynamic parameters of pentamethyl benzene using DFT study, Chem. Phys. Impact 7 (2023) 100280, https://doi.org/10.1016/j.chphi.2023.100280.
[49] Fleming, Frontier Orbitals and Organic Chemical Reactions, John Wiley & Sons, New York, 1978.
[50] I. Benjamin, AD. Udoikono, H. Louis, EC. Agwamba, TO. Unimuke, AE. Owen, AS. Adeyinka, Antimalarial potential of naphthalene-sulfonic acid derivatives: molecular electronic properties, vibrational assignments, and *in-silico* molecular docking studies, J. Mol. Struct. 1264 (2022) 133298, https://doi.org/10.1016/j.molstruc.2022.133298.
[51] G. Vijayakumari, N. Iyandurai, A. Thamarai, JM. Khaled, G. Abbas, S. Muthu, Effect of different solvent role, intermolecular forces, allergies and inflammations receptors (H1R & GPCRs) interactions of (2R)-2-{2-[(1R)-1-(4-chlorophenyl)-1-phenylethoxy] ethyl}-1-ethylpyrrolidine, J. Mol. Liq. 386 (2023) 122552, https://doi.org/10.1016/j.molliq.2023.122552.
[52] X.U. Jing-Liang, W.U. Jun, W.A.N.G. Zhi-Chun, W.A.N.G. Kun, L.I. Meng-Ying, J.-D. JIANG, H.E. Jian, L.I. Shun-Peng, Isolation and characterization of a methomyl-degrading Paracoccus sp. mdw-1, Pedosphere 19 (2) (2009) 238–243, https://doi.org/10.1016/S1002-0160(09)60113-2.
[53] C. Zhang, Z. Yang, W. Jin, X. Wang, Y. Zhang, S. Zhu, X. Yu, G. Hu, Q. Hong, Degradation of methomyl by the combination of Aminobacter sp. MDW-2 and Afipia sp. MDW-3, Lett. Appl. Microbiol. 64 (4) (2017) 289–296, https://doi.org/10.1111/lam.12715.
[54] J. Zhou, L. Zhu, J. Chen, W. Wang, R. Zhang, Y. Li, Q. Zhang, W. Wang, Degradation mechanism for Zearalenone ring-cleavage by Zearalenone hydrolase RmZHD: a QM/MM study, Sci. Total Environ. 709 (2020) 135897, https://doi.org/10.1016/j.scitotenv.2019.135897.
[55] H. Louis, GE. Mathias, TO. Unimuke, W. Emori, L. Ling, AE. Owen, AS. Adeyinka, TN. Ntui, C-Ru Cheng, Isolation, characterization, molecular electronic structure investigation, and *in-silico* modeling of the anti-inflammatory potency of trihydroxystilbene, J. Mol. Struct. 1266 (2022) 133418, https://doi.org/10.1016/j.molstruc.2022.133418.
[56] Z. Wang, Q. Zhang, G. Wang, W. Wang, Q. Wang, Hydrolysis mechanism of carbamate methomyl by a novel esterase PestE: a QM/MM approach, Int. J. Mol. Sci. 24 (1) (2022) 433, https://doi.org/10.3390/ijms24010433.
[57] J.I. Martínez-Araya, Why is the dual descriptor a more accurate local reactivity descriptor than Fukui functions? J. Math. Chem. 53 (2) (2015) 451–465, https://doi.org/10.1007/s10910-014-0437-7.
[58] S. Saravanan, V. Balachandran, Conformational stability, spectroscopic (FT-IR, FT-Raman and UV–Vis) analysis, NLO, NBO, FMO and Fukui function analysis of 4-hexylacetophenone by density functional theory, Spectrochim. Acta Part A: Mol. Biomol. Spectrosc. 138 (2015) 406–423, https://doi.org/10.1016/j.saa.2014.11.091.
[59] Z. Demircioğlu, Ç. Albayrak Kaştaş, O. Büyükgüngör, The spectroscopic (FT-IR, UV–vis), Fukui function, NLO, NBO, NPA and tautomerism effect analysis of (E)-2-[(2-hydroxy-6-methoxybenzylidene) amino] benzonitrile, Spectrochim. Acta Part A: Mol. Biomol. Spectrosc. 139 (2015) 539–548, https://doi.org/10.1016/j.saa.2014.11.078.
[60] K. Arulaabaranam, G. Mani, S. Muthu, Computational assessment on wave function (ELF, LOL) analysis, molecular confirmation and molecular docking explores on 2-(5-Amino-2-Methylanilino)-4-(3-pyridyl) pyrimidine, Chem. Data Collect. 29 (2020) 100525, https://doi.org/10.1016/j.cdc.2020.100525.
[61] N. Issaoui, H. Ghalla, S.A. Brandán, F. Bardak, H.T. Flakus, A. Atac, B. Oujia, Experimental FTIR and FT-Raman and theoretical studies on the molecular structures of monomer and dimer of 3-thiopheneacrylic acid, J. Mol. Struct. 1135 (2017) 209–221, https://doi.org/10.1016/j.molstruc.2017.01.074.
[62] F. Akman, A. Demirpolat, A.S. Kazachenko, A.S. Kazachenko, N. Issaoui, Molecular structure, electronic properties, reactivity (ELF, LOL, and Fukui), and NCI-RDG studies of the binary mixture of water and essential oil of Phlomis bruguieri, Molecules 28 (6) (2022) 2684, https://doi.org/10.3390/molecules28062684.
[63] T. Lu, Q. Chen, Interaction region indicator: a simple real space function clearly revealing both chemical bonds and weak interactions, Chem.-Methods 1 (5) (2021) 231–239, https://doi.org/10.1002/cmtd.202100007.
[64] A. Lagunin, A. Stepanchikova, D. Filimonov, V. Poroikov, PASS: prediction of activity spectra for biologically active substances, Bioinformatics 16 (8) (2000) 747–748, https://doi.org/10.1093/bioinformatics/16.8.747. PMID: 11099264.
[65] M. Hagar, HA. Ahmed, G. Aljohani, OA. Alhaddad, Investigation of some antiviral N-heterocycles as COVID 19 drug: molecular docking and DFT calculations, Int. J. Mol. Sci. 21 (11) (2020) 3922, https://doi.org/10.3390/ijms21113922.
[66] GM. Morris, R. Huey, W. Lindstrom, MF. Sanner, RK. Belew, DS. Goodsell, AJ. Olson, AutoDock4 and AutoDockTools4: automated docking with selective receptor flexibility, J. Comput. Chem. 30 (16) (2009) 2785–2791, https://doi.org/10.1002/jcc.21256.
[67] Schrödinger, L., & DeLano, W. (PyMOL. Retrieved from http://www.pymol.org/pymol (2020).
[68] K. Tabti, H. Hajji, A. Sbai, H. Maghat, M. Bouachrine, T. Lakhlifi, Identification of a potential thiazole inhibitor against biofilms by 3D QSAR, molecular docking, DFT analysis, MM-PBSA binding energy calculations, and molecular dynamics simulation, Phys. Chem. Res. 11 (2) (2023) 369–389, https://doi.org/10.22036/pcr.2022.335657.2068.
[69] I. Benjamin, H. Louis, FO. Ekpen, TE. Gber, ME. Gideon, I. Ahmad, TO. Unimuke, NP. Akanimo, H. Patel, IJ. Eko, O. Simon, EC. Agwamba, EU. Ejiofor, Modeling the anti-methicillin-resistant *Staphylococcus aureus* (MRSA) activity of (E)-6-chloro-N^2-phenyl-N^4-(4-phenyl-5-(phenyl diazinyl)-2λ^3, 3 λ^2- thiazol-2-yl)-1, 3, 5-triazine-2,4- diamine, Polycycl. Aromat. Compd. 43 (9) (2023) 7942–7969, https://doi.org/10.1080/10406638.2022.2160773.
[70] G. Salgado-Moran, V. Wilson Cardona, L. Gerli-Candia, L.H. Mendoza-Huizar, T. Abdizadeh, Identification of novel coumarin based compounds as potential inhibitors of the 3-chymotrypsin-like main protease of Sars-Cov-2 using DFT, molecular docking and molecular dynamics simulation studies, J. Chil. Chem. Soc. 67 (2) (2022) 5521–5536, https://doi.org/10.4067/s0717-97072022000205521.